Anterior expansion and posterior addition to the notochord mechanically coordinate embryo axis elongation

Susannah B.P. McLaren[1] and Benjamin J. Steventon[1]

[1] Department of Genetics, University of Cambridge, United Kingdom

Keywords:
Multi-tissue; morphogenesis; mechanics; somitogenesis; notochord; vacuolation

Summary statement:
We show that cell expansion within the notochord contributes to the elongation of segmented tissue required for embryo anterior-posterior axis extension.

Abstract

How force generated by the morphogenesis of one tissue impacts the morphogenesis of other tissues to achieve an elongated embryo axis is not well understood. The notochord runs along the length of the somitic compartment and is flanked on either side by somites. Vacuolating notochord cells undergo a constrained expansion, increasing notochord internal pressure and driving its elongation and stiffening. Therefore, the notochord is appropriately positioned to play a role in mechanically elongating the somitic compartment. We use multi-photon cell ablation to remove specific regions of the notochord and quantify the impact on axis elongation. We show that anterior expansion generates a force that displaces notochord cells posteriorly relative to adjacent axial tissues, contributing to the elongation of segmented tissue during post-tailbud stages. Unexpanded cells derived from progenitors at the posterior end of the notochord provide resistance to anterior notochord cell expansion, allowing for stress generation along the AP axis. Therefore, notochord cell expansion beginning in the anterior, and addition of cells to the posterior notochord, act as temporally coordinated morphogenetic events that shape the zebrafish embryo AP axis.

Introduction

Elongation of the embryo anterior-posterior (AP) axis requires the physical deformation of multiple axial tissues as they undergo morphogenesis (Bénazéraf et al., 2017; Steventon et al., 2016; Xiong et al., 2020). The vertebrate embryo body axis is segmented into blocks of tissue called somites, that later form the skeletal muscle and vertebrae of the adult body (Gomez et al., 2008). Running through the middle of the embryo, the rod-shaped notochord is flanked on either side by the somitic compartment: the somites in the segmented region of the axis and the presomitic mesoderm in the posterior (Fig. 1A and B) (Stemple, 2005).

Mutants lacking a notochord have fused somites (Talbot et al., 1995), and disruption of notochord morphogenesis results in axis truncation and skeletal malformations (Bagwell et al., 2020; Ellis et al., 2013). Studies in Xenopus embryos have identified the circumferentially constrained expansion of cells within the notochord sheath to lead to an increase in notochord stiffness as the embryo develops, making it a candidate for driving the physical deformation of surrounding somitic tissue that may be required for AP axis elongation (Adams et al., 1990; Koehl et al., 2000). In the zebrafish notochord, cells differentiate into either a sheath or vacuolated cell type (Yamamoto et al., 2010). Vacuolating notochord cells expand over time as they draw in fluid, as in Xenopus (Fig.1C) (Ellis et al., 2013), and notochord volume increases as development progresses (Steventon et al., 2016). However, it remains unclear how force generated by notochord morphogenesis impacts the elongation of the somitic compartment and extends the zebrafish embryo AP axis.

Concomitant with notochord cell expansion, a separate morphogenetic event occurs in which cells are contributed to the posterior end of the notochord from a population of notochord progenitors (Fig.1C) (Kanki and Ho, 1997). Early termination of progenitor addition to the notochord is associated with AP axis elongation defects (Row et al., 2016). Whilst the role of other tailbud-located progenitor populations in elongating the AP axis has been investigated (Goto et al., 2017; Mongera et al., 2018; Attardi et al., 2018), it is not known how the posterior contribution of cells from notochord progenitors is coordinated with the expansion of more anterior notochord cells, and how these combined processes impact axis elongation.

As notochord morphogenesis progresses somites are segmented from the unsegmented presomitic mesoderm in the posterior tailbud until 30 to 34 somites are formed in total, with the tailbud remaining present until the 30-somite stage when it begins to degenerate (Fig.1A) (Gomez et al., 2008; Oates et al., 2012; Kimmel et al., 1995). As somites mature, they undergo bending until a 'chevron shape' is reached (Rost et al., 2014). Whilst elongation generated from unsegmented tailbud-derived tissue has been studied (Das et al., 2019; Dray et al., 2013; Lawton et al., 2013; Mongera et al., 2018; Steventon et al., 2016), how elongation progresses in mature segmented tissue during post-tailbud stages of development is less clear.

Here, we utilise targeted multi-photon tissue ablation to investigate the physical impact of notochord morphogenesis on the surrounding somitic compartment, and identify the concomitant expansion of notochord cells, and contribution of progenitors to the posterior end of the notochord, as two temporally coordinated morphogenetic events that shape the zebrafish embryo AP axis.

Results and Discussion

Modes of axis elongation change as embryos progress from tailbud stages into post-tailbud stages of development

To quantitatively characterise AP axis elongation occurring concomitantly with notochord volume increase, we live-imaged developing zebrafish embryos as notochord cell expansion was progressing and quantified elongation in segmented and unsegmented regions of the axis (Fig. S1A, B and movie 1). Segmented tissue elongation is tracked using the boundaries of 5-formed somites and segmentation-derived elongation is tracked using the presomitic mesoderm and somites formed as development progresses (Fig.1A).

We compared elongation over a 5-hour period during tailbud (24ss) and post-tailbud stages (30ss) to investigate the modes of axis elongation utilised during each of these phases of embryo morphogenesis. No significant increase in segmented tissue length was measured during tailbud stages (Fig.1D and S1A). However, in post-tailbud stages mean segmented tissue length increased by approximately 13%

(Fig.1D and S1B). In contrast, less segmentation-derived elongation was measured in post-tailbud stages compared to tailbud-stage embryos (Fig.1E and S1A and B). These findings show that embryo AP axis elongation can be described by two phases: segmentation-derived elongation during tailbud stages, followed by elongation of segmented tissue during post-tailbud stages (Movie 1).

Notochord cell expansion leads to the posterior displacement of notochord cells relative to adjacent axial tissues

To gain insight into how notochord morphogenesis impacts axis elongation during tailbud and post-tailbud stages of development, we characterised notochord cell expansion both temporally, in an equivalent region of the notochord of different stage embryos (Fig.S2A), and spatially, in notochord regions in the anterior versus the posterior in embryos of the same stage (Fig.S2B). In agreement with previous work, we observed that vacuolating notochord cells expanded over time (Bagwell et al., 2020; Dale and Topczewski, 2011; Yamamoto et al., 2010) (Fig.1F), with the earlier onset of vacuolation in the anterior notochord likely leading to larger cell lengths in the anterior versus posterior (Fig.1G). Photolabelling stripes along the axis in embryos entering post-tailbud stages revealed that anterior vacuolated notochord cells move posteriorly relative to adjacent regions of somitic compartment and neural tube (Fig. 2A), with the shift between notochord cells and adjacent tissues being smaller in the posterior region of the axis where notochord cells are unexpanded and undifferentiated (Fig.2B, C and S3).

To investigate how forces generated from anterior notochord cell expansion might propagate along the AP axis and to neighbouring tissues, a technique is required that allows for precise spatio-temporal removal of notochord cells. We used multi-photon ablation to cut through notochord cells at defined regions of the AP axis (Movie 2), resulting in the destruction of tissue local to the ablation site and minimal damage to adjacent tissues such as the Shh expressing floor plate lying immediately dorsal to the notochord (Fig.2D). Ablations were performed at the onset of vacuolation, removing cells before water uptake and subsequent expansion (Fig. S2C). Ablation of anterior notochord cells reversed the direction of displacement of expanding vacuolated cells posterior to the ablation site (Figs.2E-G, and movie 3),

and over longer timescales the ablated region eventually closes - possibly aided by changes in cell packing (Norman et al., 2018) (Movie 4). However, the movement of unexpanded notochord cells in the posterior undifferentiated region was less affected (Fig. 2H). Thus, the expansion of vacuolated notochord cells, beginning in the anterior and progressing posteriorly along the notochord, generates a force displacing neighbouring expanded notochord cells posteriorly relative to adjacent axial tissues in post-tailbud stage embryos.

Notochord cell expansion is a driver of segmented tissue elongation during post-tailbud stages of development

We observed that elongation during tailbud stages was associated with the segmentation of posterior unsegmented tissue. To investigate whether notochord cell expansion impacted this mode of elongation, we performed site-specific ablations of anterior notochord cells at the onset of vacuolation and measured posterior tail elongation during tailbud stages of development (Fig.3A and B). Posterior tail elongation was not significantly affected in ablated embryos (Fig.3C and D). Strikingly, segmentation-derived elongation could continue in an embryo with an ablation extending into the posterior notochord (Movie 5), and presomitic mesoderm progenitors continued to exit the tailbud in ablated embryos (Fig.S4A). Together, these results demonstrate that segmentation-derived elongation is a robust process that can continue in the absence of notochord cell expansion.

To investigate whether notochord cell expansion impacts the segmented tissue elongation observed during post-tailbud stages, we measured the length of a 5-somite region from the 30-somite stage over a 5-hour period in embryos with and without anterior notochord ablations. The region used for quantifying segmented tissue elongation was located in an equivalent region along the axis in control and ablated embryos and positioned posteriorly away from the site of notochord ablation in the ablated case (Fig. 3E). As characterised above, this region was adjacent to either posteriorly directed notochord cell movement (control) or anteriorly directed notochord cell movement (ablated). Segmented tissue elongation was approximately halved in ablated embryos (Figs.3F-H, and movie 6), and inhibiting vacuolation with

Bafilomycin (Ellis et al., 2013) had an even greater effect, blocking elongation of segmented tissue (Figs.3I, S4B-D). Together these results reveal a role for notochord cell expansion in elongating segmented tissue in post-tailbud stage embryos.

Notochord progenitors provide a source of resistance to anterior notochord cell expansion that facilitates the elongation of segmented tissue

Unexpanded notochord cells in the posterior exhibited less movement relative to adjacent tissues than anterior expanded cells, suggesting that they may resist the force generated by cell expansion. We therefore hypothesised that expanding vacuolated notochord cells push against unexpanded posterior notochord cells, generating a stress along the axis that contributes to segmented tissue elongation. We first determined if the addition of unexpanded cells to the posterior notochord was coordinated with the progression of notochord cell expansion posteriorly along the axis. Using *Noto* expression to mark the notochord progenitor domain, we found that notochord progenitor domain volume decreased as development progressed (Fig. S5A and C), corresponding to a decrease in the length contributed to the posterior end of the notochord by progenitors (Fig. S5B and D). Next, we attempted to prevent the contribution of cells to the posterior notochord by ablating the notochord progenitor population (Fig. S5E). Whilst axis elongation defects occurred (Fig. S5F), the notochord progenitor pool was able to recover after ablation and re-form the posterior notochord (Figs. S5H and I). Intriguingly, elongation resulting from the segmentation of the final few somites in the region where the posterior notochord had been recovered was unaffected (Figs. S5G and J). These findings highlight the robustness of posterior processes that contribute to axis elongation, both in terms of cell contribution to the posterior notochord and segmentation-derived elongation.

Given that the notochord re-formed after notochord progenitor ablation, we decided to focus our perturbations on the already formed posterior notochord. In embryos entering post-tailbud stages of development notochord cell expansion has progressed posteriorly along the axis to the anterior tail region (close to the end of the yolk extension) where it meets the unexpanded notochord cells (Fig.S6C). To investigate whether unexpanded notochord cells are subject to a force generated by

anterior notochord cell expansion, we imaged the nuclei of unexpanded notochord cells in this region in control embryos, and just posterior to an ablation site in ablated embryos (Fig. 4A). Nuclei in control embryos were angled towards the posterior, whereas nuclei posterior to an ablation site were angled towards the anterior (Fig.4B and S6A), suggesting that unexpanded notochord cells are being deformed by a posteriorly directed force arising from notochord cell expansion.

To investigate whether unexpanded posterior notochord cells provided a source of resistance to notochord cell expansion, we ablated these cells in embryos at post-tailbud stages and manually tracked expanding notochord cells just anterior to the ablation site (Figs. 4C, D and S6C). The posterior displacement of expanding cells was increased in ablated embryos compared to controls (Fig. 4G and movie 7), suggesting that posterior notochord cells do provide a source of resistance. We investigated notochord cell adhesion to the sheath surrounding the notochord as a potential source of this resistance. Visualising the cell-extracellular matrix (ECM) adhesion protein vinculin revealed that vinculin puncta were located at the interface between notochord cells and the surrounding sheath in the posterior, whilst far fewer puncta were observed at this interface in the anterior where notochord cells are expanded (Fig. 4E and S6B). Finally, we found the elongation of somites located anterior to the posterior notochord ablation site (Fig. 4C) was decreased (Figs. 4F and H). These findings suggest that posterior unexpanded notochord cells provide a source of resistance to notochord cell expansion that facilitates the elongation of segmented tissue in post-tailbud stage embryos.

Our findings show that, whilst segmentation-derived axis elongation can progress independently of notochord cell expansion, this expansion plays a key role in elongating segmented tissue during later stages of embryo development, in agreement with phenotypes observed in embryos with defective notochord vacuolation (Sun et al., 2020). Physical coupling between notochord cells and the somitic compartment is thought to be stronger in the posterior versus the anterior of the embryo (Dray et al. 2013; Tlili et al. 2019), and the resulting impact of this is observed in the larger displacement between these tissues in anterior regions where notochord cells have expanded and smaller displacement in posterior regions where expansion is yet to occur (Figs. 2A-C). Physical coupling is likely facilitated by a shared ECM-interface between the notochord and somitic compartment (Guillon et al., 2020), with a higher number of vinculin puncta present at this interface in the

posterior and lower number in the anterior (Fig. 4E). We therefore propose a model in which the progression of vacuolation posteriorly along the notochord leads to the posterior displacement of expanded (vacuolated) notochord cells that is resisted by unexpanded cells in the posterior undifferentiated notochord (Fig.4I). As expanding notochord cells push on the posterior notochord, coupling between the notochord and somitic compartment in the posterior would facilitate stress transmission to the segmented tissue located anterior to the coupled region (Fig.4J). Over time the posterior notochord region resisting the push from expanding notochord cells will shrink, as vacuolation progresses along the notochord and notochord progenitors are depleted (Fig.4I), facilitating stress transmission to more and more posterior regions of the somitic compartment as development progresses.

In summary, we highlight the importance of considering multi-tissue mechanical interactions in mechanisms of embryo axis elongation and report a role for notochord cell expansion in mediating the elongation of somites. Further studies investigating whether force generated by notochord cell expansion acts to directly stretch myofibers, or impacts myofiber differentiation and elongation via indirect mechanochemical regulation, will deepen our understanding of these multi-tissue interactions.

Acknowledgements
We thank Andrea Dimitracopoulos, Fengzhu Xiong and Bertrand Benazeraf for critical reading of the manuscript, and members of the Steventon, Martinez-Arias and Franze group meetings for their support and feedback on the project. We thank Ben Martin's lab for the kind gift of the Ntl:kaede line. We also thank the PDN fish facility for their unwavering help and support with animal care and maintenance, and the Cambridge Advanced Imaging Centre for their support with laser ablation experiments. B.S. was supported by a Henry Dale Fellowship jointly funded by the Wellcome Trust and the Royal Society (109408/Z/15/Z) and S.B.P.M. was supported by the Wellcome Trust funded Developmental Mechanisms PhD programme.

Author Contributions
S.B.P.M. and B.S. conceived the project. S.B.P.M. carried out experiments and analysed the data. S.B.P.M. and B.S. wrote the manuscript.

Competing Interests
The authors declare no competing interests.

References

Adams, D. S., Keller, R. and Koehl, M. A. (1990). The mechanics of notochord elongation, straightening and stiffening in the embryo of Xenopus laevis. *Development* **110**, 115–130.

Attardi, A., Fulton, T., Florescu, M., Shah, G., Muresan, L., Lenz, M. O., Lancaster, C., Huisken, J., van Oudenaarden, A. and Steventon, B. (2018). Neuromesodermal progenitors are a conserved source of spinal cord with divergent growth dynamics. *Development* **145**, dev166728.

Bagwell, J., Norman, J., Ellis, K., Peskin, B., Hwang, J., Ge, X., Nguyen, S. V., McMenamin, S. K., Stainier, D. Y. and Bagnat, M. (2020). Notochord vacuoles absorb compressive bone growth during zebrafish spine formation. *Elife* **9**, 1840.

Bénazéraf, B., Beaupeux, M., Tchernookov, M., Wallingford, A., Salisbury, T., Shirtz, A., Shirtz, A., Huss, D., Pourquié, O., Francois, P., et al. (2017). Multi-scale quantification of tissue behavior during amniote embryo axis elongation. *Development* **144**, 4462–4472.

Choi, H. M. T., Beck, V. A. and Pierce, N. A. (2014). Next-generation in situ hybridization chain reaction: higher gain, lower cost, greater durability. *ACS Nano* **8**, 4284–4294.

Dale, R. M. and Topczewski, J. (2011). Identification of an evolutionarily conserved regulatory element of the zebrafish col2a1a gene. *Developmental Biology* **357**, 518–531.

Das, D., Jülich, D., Schwendinger-Schreck, J., Guillon, E., Lawton, A. K., Dray, N., Emonet, T., O'Hern, C. S., Shattuck, M. D. and Holley, S. A. (2019). Organization of Embryonic Morphogenesis via Mechanical Information. *Developmental Cell*.

Dray, N., Lawton, A., Nandi, A., Jülich, D., Emonet, T. and Holley, S. A. (2013). Cell-fibronectin interactions propel vertebrate trunk elongation via tissue mechanics. *Curr. Biol.* **23**, 1335–1341.

Ellis, K., Bagwell, J. and Bagnat, M. (2013). Notochord vacuoles are lysosome-related organelles that function in axis and spine morphogenesis. *The Journal of Cell Biology* **200**, 667–679.

Gomez, C., Özbudak, E. M., Wunderlich, J., Baumann, D., Lewis, J. and Pourquié, O. (2008). Control of segment number in vertebrate embryos. *Nature* **454**, 335–339.

Goto, H., Kimmey, S. C., Row, R. H., Matus, D. Q. and Martin, B. L. (2017). FGF and canonical Wnt signaling cooperate to induce paraxial mesoderm from tailbud neuromesodermal progenitors through regulation of a two-step epithelial to mesenchymal transition. *Development* **144**, 1412–1424.

Guillon, E., Das, D., Jülich, D., Hassan, A.-R., Geller, H. and Holley, S. (2020). Fibronectin is a smart adhesive that both influences and responds to the mechanics of early spinal column development. *eLife*

Kanki, J. P. and Ho, R. K. (1997). The development of the posterior body in zebrafish. *Development* **124**, 881–893.

Kimmel, C. B., Ballard, W. W., Kimmel, S. R., Ullmann, B. and Schilling, T. F. (1995). Stages of embryonic development of the zebrafish. *Dev. Dyn.* **203**, 253–310.

Koehl, M., Quillin, K. J., Pell, C. A. (2000) Mechanical Design of Fiber-Wound Hydraulic Skeletons: The Stiffening and Straightening of Embryonic Notochords. *Amer. Zool.* **40,** 28-41

Lawton, A. K., Nandi, A., Stulberg, M. J., Dray, N., Sneddon, M. W., Pontius, W., Emonet, T. and Holley, S. A. (2013). Regulated tissue fluidity steers zebrafish body elongation. *Development* **140**, 573–582.

Mongera, A., Rowghanian, P., Gustafson, H. J., Shelton, E., Kealhofer, D. A., Carn, E. K., Serwane, F., Lucio, A. A., Giammona, J. and Campàs, O. (2018). A fluid-to-solid jamming transition underlies vertebrate body axis elongation. *Nature* **561**, 401–405.

Norman, J., Sorrell, E. L., Hu, Y., Siripurapu, V., Garcia, J., Bagwell, J., Charbonneau, P., Lubkin, S. R. and Bagnat, M. (2018). Tissue self-organization underlies morphogenesis of the notochord. *Phil.I Trans. R. Soc. B* **373**

Oates, A. C., Morelli, L. G. and Ares, S. (2012). Patterning embryos with oscillations: structure, function and dynamics of the vertebrate segmentation clock. *Development* **139**, 625–639.

Rost, F., Eugster, C., Schröter, C., Oates, A. C. and Brusch, L. (2014). Chevron formation of the zebrafish muscle segments. *Journal of Experimental Biology* **217**, 3870–3882.

Row, R. H., Tsotras, S. R., Goto, H. and Martin, B. L. (2016). The zebrafish tailbud contains two independent populations of midline progenitor cells that maintain long-term germ layer plasticity and differentiate in response to local signalling cues. *Development* **143**, 244–254.

Stemple, D. L. (2005). Structure and function of the notochord: an essential organ for chordate development. *Development* **132**, 2503–2512.

Steventon, B., Duarte, F., Lagadec, R., Mazan, S., Nicolas, J.-F. and Hirsinger, E. (2016). Species-specific contribution of volumetric growth and tissue convergence to posterior body elongation in vertebrates. *Development* **143**, 1732–1741.

Sun, X., Zhou, Y., Zhang, R., Wang, Z., Xu, M., Zhang, D., Huang, J., Luo, F., Li, F., Ni, Z., et al. (2020). Dstyk mutation leads to congenital scoliosis-like vertebral malformations in zebrafish via dysregulated mTORC1/TFEB pathway. *Nat Comm* **11**, 1–17.

Talbot, W. S., Trevarrow, B., Halpern, M. E., Melby, A. E., Farr, G., Postlethwait, J. H., Jowett, T., Kimmel, C. B. and Kimelman, D. (1995). A homeobox gene essential for zebrafish notochord development. *Nature* **378**, 150–157.

Tlili, S., Yin, J., Rupprecht, J. F., Mendieta-Serrano, M. A., Weissbart, G., Verma, N., Teng, X., Toyama, Y., Prost, J. and Saunders, T. E. (2019). Shaping the zebrafish myotome by intertissue friction and active stress. *Proc Natl Acad Sci USA* **116**, 25430–25439.

Xiong, F., Ma, W., Bénazéraf, B., Mahadevan, L. and Pourquié, O. (2020). Mechanical Coupling Coordinates the Co-elongation of Axial and Paraxial Tissues in Avian Embryos. *Developmental Cell* **55**, 1-13.

Yamamoto, M., Morita, R., Mizoguchi, T., Matsuo, H., Isoda, M., Ishitani, T., Chitnis, A. B., Matsumoto, K., Crump, J. G., Hozumi, K., et al. (2010). Mib-Jag1-Notch signalling regulates patterning and structural roles of the notochord by controlling cell-fate decisions. *Development* **137**, 2527–2537.

Materials and Methods

Zebrafish strains and maintenance

This research was regulated under the Animals (Scientific Procedures) Act 1986 Amendment Regulations 2012 following ethical review by the University of Cambridge Animal Welfare and Ethical Review Body (AWERB).
Adult Zebrafish (Danio rerio) and embryos were reared at 28°C and staged using the number of somites. Wildtype embryos used in this study were of the TL strain. Prior to live imaging embryos were anaesthetised with tricaine (MS-222).
The following zebrafish lines were used in this study; H2B-GFP, Tg(actb2:Lifeact-EGFP), and pNtl:Kaede[16].

Tailbud stages correspond to the stages during the segmentation period after a tailbud has been formed, post-tailbud stages correspond to the pharyngula period, when the tailbud has started to degenerate (Kimmel et al., 1995).

Timelapse Live Imaging

Embryos were mounted in 3% Methylcellulose to hold embryos still whilst allowing movement of the tail and ensuring embryos could continue to develop normally. Embryos were mounted in glass bottom dishes (MatTek), with the head and yolk submerged in methylcellulose but with the tail freed of methylcellulose. Embryos were submerged in E3 media and an eyelash tool was used to reposition embryos in the methylcellulose so that they were lying flat on the bottom of the dish. Dishes with mounted embryos were transferred to a Zeiss LSM 700 confocal microscope

equipped with a heated chamber set to 28°C. A 10x air objective (NA=0.45) was used to capture the whole body of developing embryos for timelapse movies.

Drug treatments

Bafilomycin A1 (Sigma Aldrich) (an inhibitor of vacuolar type H^+-ATPases required for vacuole expansion) was used to inhibit vacuolation in the notochord of developing zebrafish embryos. 16ss embryos were submerged in E3 media with Bafilomycin at a final concentration of 0.5uM. Embryos were then incubated for 6 hours at 28°C. Vacuolation in the notochord of Lifeact-GFP embryos was imaged live using a 20x air objective. Live imaging of somite elongation in DMSO and Bafilomycin treated embryos was performed using pNtl:kaede-expressing embryos pre-treated with 0.25µM Bafilomycin (or DMSO of an equivalent volume) and imaged from the 30-somite stage using a multi-well chamber.

Photolabelling

Wild-type Zebrafish embryos were injected with approximately 200 pg of nuclear-targeted Kikume at the one-cell stage and incubated in the dark. Embryos were mounted in glass bottom dishes and transferred to the microscope as described above for live imaging. To investigate the movement of notochord cells relative to adjacent regions of the somitic compartment and neural tube, rectangular stripes were defined at different points along the embryo. The distance between the anterior extent of labels made in each tissue was used to measure the relative shift (Fig. S3). Photoconversion of NLS-KikGR was performed whilst using a 20x air objective and scanning the 405 nm laser at 11% power within defined regions. Photolabelling was confirmed by simultaneously visualing both NLS-KikGR emissions using the 488 nm and 561nm lasers.

Cell tracking

The centre of notochord cells in lifeact-GFP expressing embryos was manually tracked in imaris relative to a nearby somite boundary located in an equivalent region of the axis in each embryo. Reference frames were generated using the ‘reference frame’ tool, the x axis was aligned with the AP axis and the origin was placed at the somite boundary.

Hybridisation Chain Reaction (HCR)

HCR was used to visualise gene expression in fixed embryos. HCR has previously been described here (Choi et al., 2014). The notochord progenitor domain was visualised using probes targeted to the gene *Noto* (also known as *flh*).

Immunohistochemistry

Embryos were fixed in 4% paraformaldehyde overnight at 4ºC. Embryos were then washed and blocked in 4% goat serum in PBDT before incubating overnight at 4ºC with primary antibody anti-vinculin (ab91459, abcam) at 1:200 in 4% goat serum in

PBDT. Secondary antibodies were also incubated overnight at 1:500 in 4% goat serum in PBDT.

Photoablation

Laser ablation was performed using a TriM Scope II Upright 2-photon scanning fluorescence microscope equipped with a tunable near-infrared laser. Inspector Pro software was used to control the microscope and a laser power of approximately 1.3W was used for ablation.

Notochord ablations were carried out using a lifeact-GFP reporter line to visualise notochord cells and ablations were performed in the plane of the notochord. Notochord cells were ablated in either the anterior or posterior regions of the notochord in embryos at the 16-18 somite stage to ensure that cells fated to become the vacuolated cell type were destroyed before they had drawn in water and osmotically expanded. Ablations may include some undifferentiated sheath-fated cells (Yamamoto et al., 2010).

For notochord progenitor ablations the morphology of the notochord progenitor cell population was used to determine the location of the notochord progenitors. Ablations were carried out to ensure as many of the notochord progenitors as possible were ablated, without ablating any other progenitor types.

Image processing and analysis

Images were processed either in ImageJ/Fiji or Imaris.

Length and curvature measurements

For length and curvature measurements the ImageJ plug-in ‘Kappa’ was used. NLS-KikGR, H2B-GFP and Lifeact-GFP expressing embryos were used for length and curvature measurements. A maximum projection of the nuclear-GFP or actin-GFP channel was used so that somite boundaries could be visualised and used to define the segmented and unsegmented regions. Embryo side views were used to measure the curvature and length of regions of the axis. Trunk curvature was measured using points to generate a spline, and the points were adjusted so that a smooth curve fitting the curvature of the region passed through the midpoint of somites in that region. Tail curvature was measured in a similar fashion. The average curvature was used for comparing the curvature of these regions in multiple embryos of different stages. To visualise the curvature profile along the whole somitic compartment in embryos of different stages, a spline passing from the anterior tip to the posterior tip of the somitic compartment was generated, and point curvature was used to generate a heatmap in order to visualise the curvature profile along the axis.

Notochord progenitor domain volume

To measure the volume of the notochord progenitor domain at different developmental stages *Noto* (also known as *flh)* gene expression was visualised using HCR and acquisition of confocal z-stacks of fixed 20ss, 25ss, and 30ss embryo tails. These images were imported into imaris, allowing for visualisation in

3D. The ‘surfaces’ function in imaris was used to generate a surface around the *Noto* gene expression signal, with surface volume given as an output.

Vacuole AP length measurements

The ‘oblique slicer’ tool in imaris was used to find a plane that passed through the middle of the notochord where the maximum length of vacuoles could be properly visualised. The ‘measurements’ tool was used to make two points per vacuole defining a line passing through the greatest AP length of the vacuole. Line lengths were calculated using an inbuilt function in imaris. Vacuole lengths were measured in wildtype or DMSO treated Lifeact-GFP expressing embryos.

Nuclei angle measurements

The ‘measurements’ tool in imaris was used to measure the angle between nuclei located dorsally in the notochord and the dorsal AP edge of the notochord in fixed DAPI stained embryos with and without notochord ablations.

Data analysis

Data was stored in excel spreadsheets and analysis was performed using the programming language ‘Python’. All data plots were generated in Python using the ggplot library. Box plots show the median, upper and lower quartiles, and whiskers represent 1.5 times the interquartile distance. Linear regression analysis was used to fit a line to data in scatter plots showing length gained versus time. Scatter plots were generated using the geom_point function. The scikit-learn module was used for linear regression analysis. All data points were shown and included in statistical analyses.

Statistical Analysis

The Mann-Whitney U nonparametric statistical test was used to test whether two independent samples came from populations with the same distribution. This test was implemented in python using the scipy.stats.mannwhitneyu() function.
The Kruskal-Wallis nonparametric statistical test was used to test whether more than two independent samples came from populations with the same distribution. Pairwise comparisons between samples were performed in a post-hoc fashion to identify whether compared samples came from populations with the same distribution. The Kruskal-Wallis test was implemented using the stats.kruskal() function, and the post hoc test was implemented with the sp.posthoc_conover() function. In the case of segmentation-derived elongation in anterior-ablated and control embryos, a power analysis was conducted to estimate sample sizes needed to detect a difference of 3% between the means of each group at a standard power score of 0.8.
In all cases a p-value of <0.05 was taken as a threshold for significance.

Figures

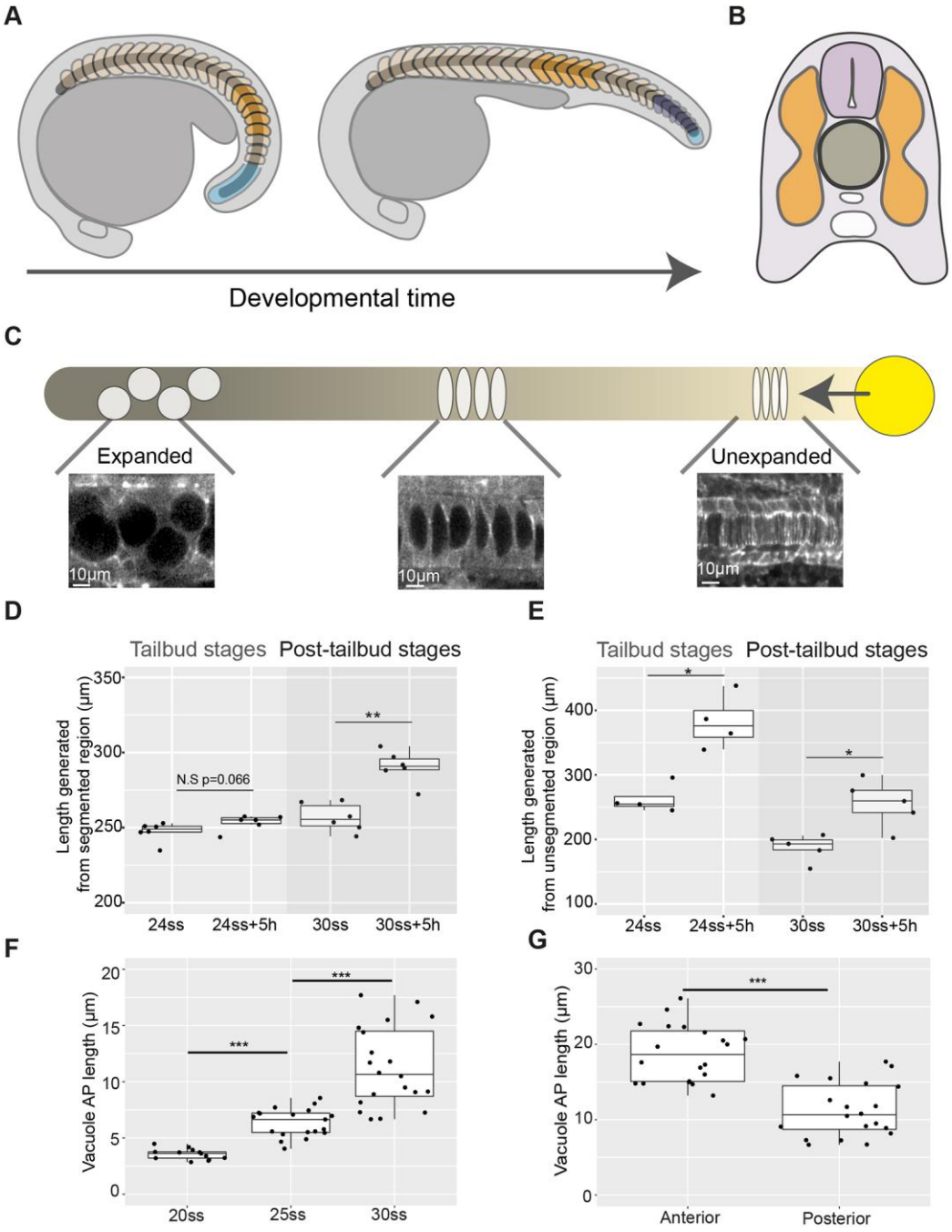

Fig. 1. Axis elongation occurs predominantly in the unsegmented region during tailbud stages and later continues in segmented tissue.

(A) Schematic outlining segmented (orange and dark-blue) and unsegmented (light-blue) regions of the somitic compartment. Dark-blue somites are formed from unsegmented tissue between the stages shown.

(B) Schematic showing axial tissues in a cross-section of the Zebrafish. The notochord (dark-grey) is flanked by the somitic compartment (orange) on either side, and the neural tube (light-purple) dorsally.
(C) Schematic outlining events in notochord morphogenesis. Vacuolation progresses from the anterior (darker) to posterior (lighter) of the notochord and progenitors expressing Noto (yellow) add cells to the notochord rod.
(D) The length of a region of segmented tissue in tailbud (24ss) and post-tailbud (30ss) embryos and length generated from this region over 5-hours (n=6 and n=6 respectively, $p>0.05$, $p<0.01$ respectively).
(E) The length of a region of unsegmented tissue in tailbud (24ss) and post-tailbud (30ss) embryos and length generated from this region over 5-hours (n=4 and n=5 respectively, $p<0.05$, $p<0.05$ respectively).
(F) AP length of vacuoles at different stages of development (n=3, n=4 and n=4 embryos per stage respectively, 3 to 5 vacuoles measured per embryo. $p<0.001$ and $p<0.001$ respectively).
(G) AP length of vacuoles in anterior and posterior regions of 30-somite stage embryos (n= 4 embryos, 5 vacuoles measured per region. $p<0.001$).
Anterior is to the left and posterior to the right in all images.

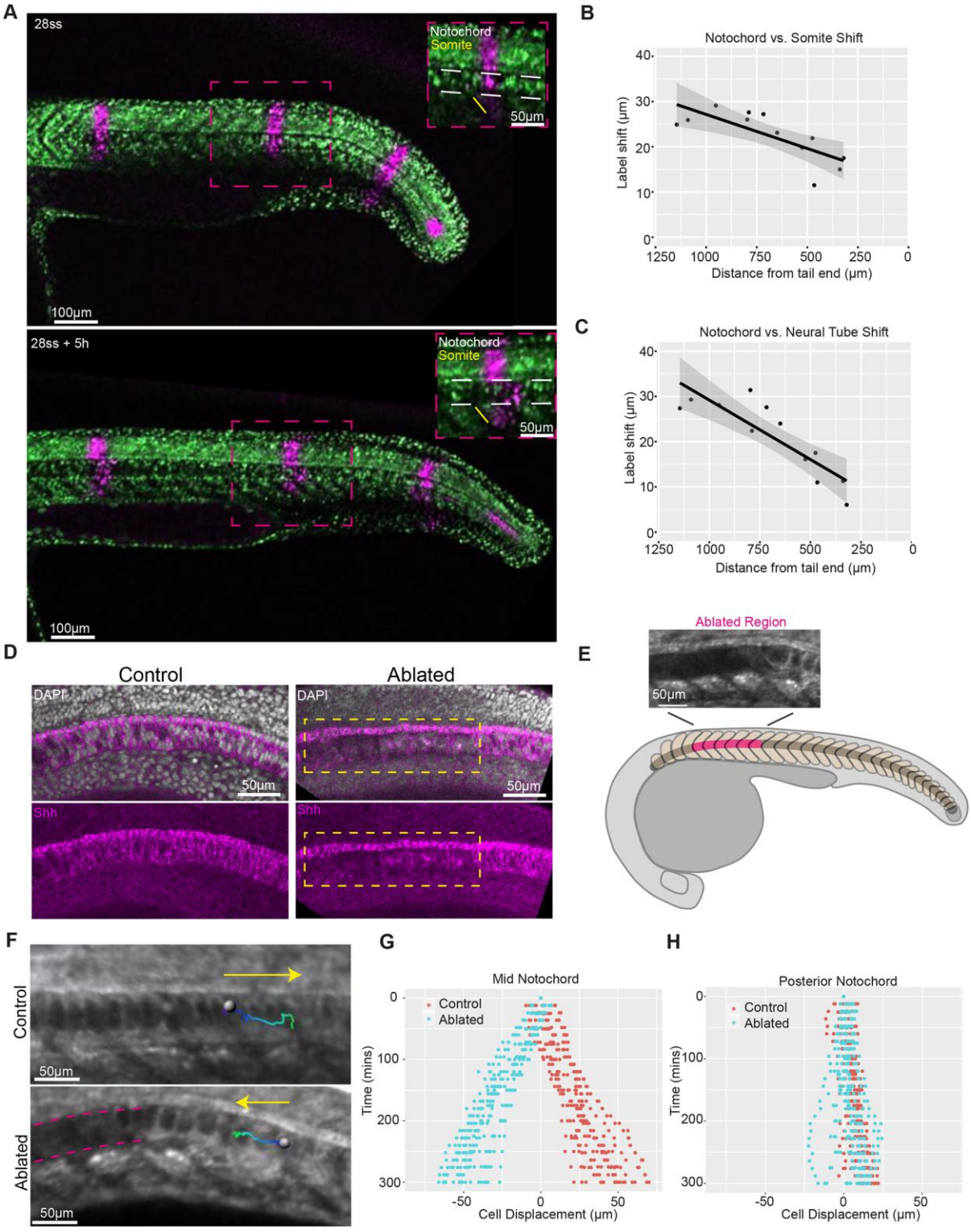

Fig. 2. Notochord cell expansion leads to the posterior displacement of notochord cells relative to adjacent axial tissues.

(A) Photolabel stripes along the length of an embryo expressing NLS-KikGR at the 28-somite stage and 5 hours later.
(B) Shift between notochord and somite photolabels versus distance from the posterior end of the embryo.

(C) Shift between notochord and neural tube photolabels versus distance from the posterior end of the embryo.
(D) DAPI and Shh expression in representative control and ablated embryos (n=4 embryos per condition).
(E) A schematic showing the ablated region in an embryo entering post-tailbud stages. Ablations were made at the onset of vacuolation.
(F) Expanding notochord cell tracks in control and ablated embryos.
(G) Displacement of manually tracked expanded notochord cells in control and ablated embryos (n=6 embryos per condition, 3 tracks per embryo).
(H) Cell displacement in μm of manually tracked unexpanded notochord cells in control and ablated embryos (n=5 embryos per condition, 3 tracks per embryo).

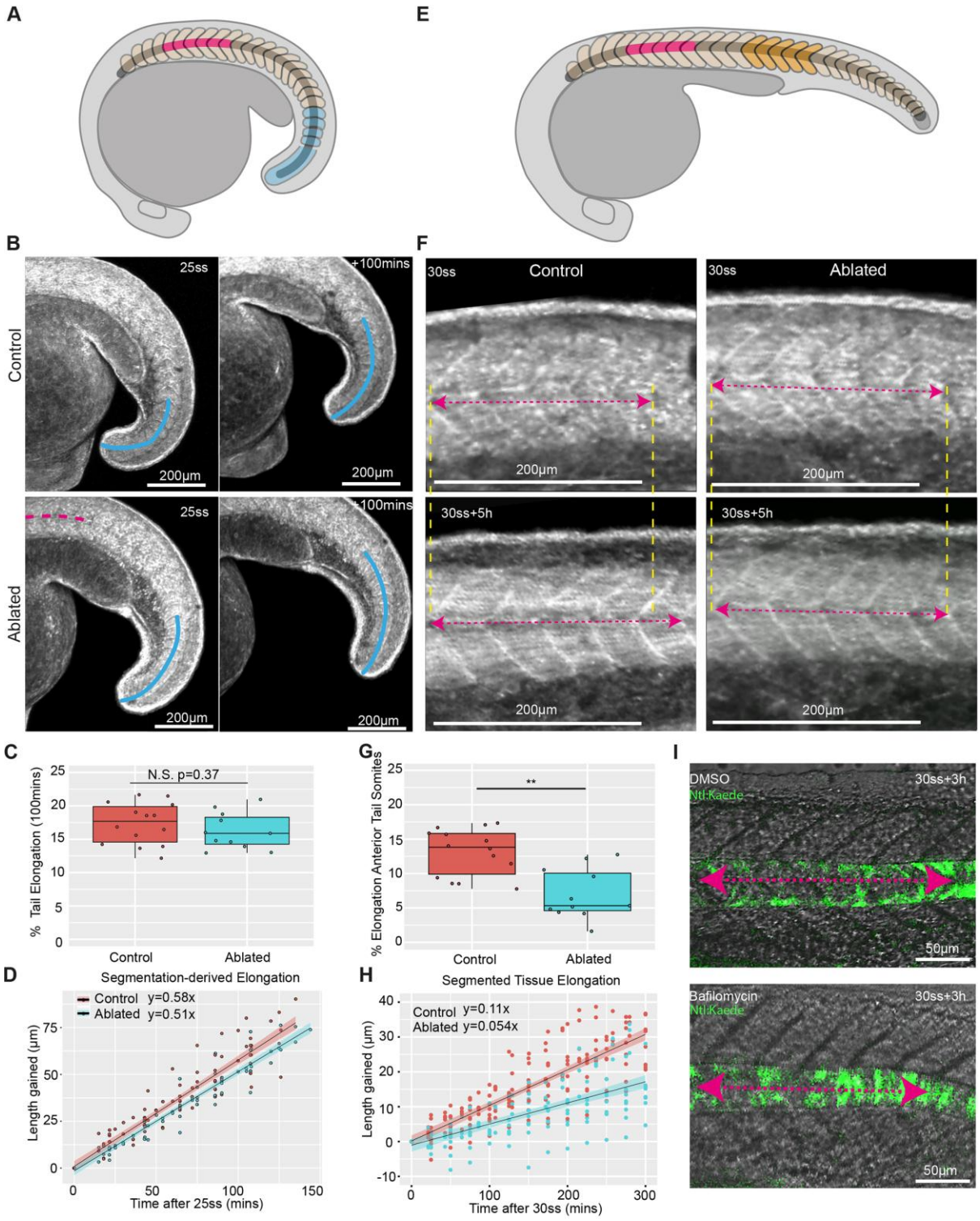

Fig. 3. Notochord cell expansion contributes to segmented tissue elongation during post-tailbud stages.

(A) Schematic showing the ablated region (magenta) and region tracked for measuring segmentation-derived elongation (blue).
(B) Control and ablated Lifeact-GFP expressing embryos imaged at the 25-somite stage and 100 minutes later. Overlaid curves show the region tracked for elongation measurements. The magenta line indicates the region where the notochord is ablated.

(C) Percentage elongation of the tail region in control and ablated embryos (n=14 control embryos, n=11 ablated embryos, p=0.37).
(D) Length gained in the posterior tail of tailbud stage control and ablated embryos over time.
(E) Schematic showing the ablated region (magenta) and region tracked for measuring segmented tissue elongation (orange).
(F) Elongation of a 5-somite region in control and ablated post-tailbud stage Lifeact-GFP expressing embryos.
(G) Percentage elongation of a 5-somite region in control and ablated post-tailbud stage embryos over a period of 5 hours (n=14 control and n=11 ablated embryos, p<0.001)
(H) Length gained in a 5-somite region in control and ablated post-tailbud stage embryos over time.
(I) Image showing the length of a 5-somite region in representative DMSO and Bafilomycin treated post-tailbud stage embryos.

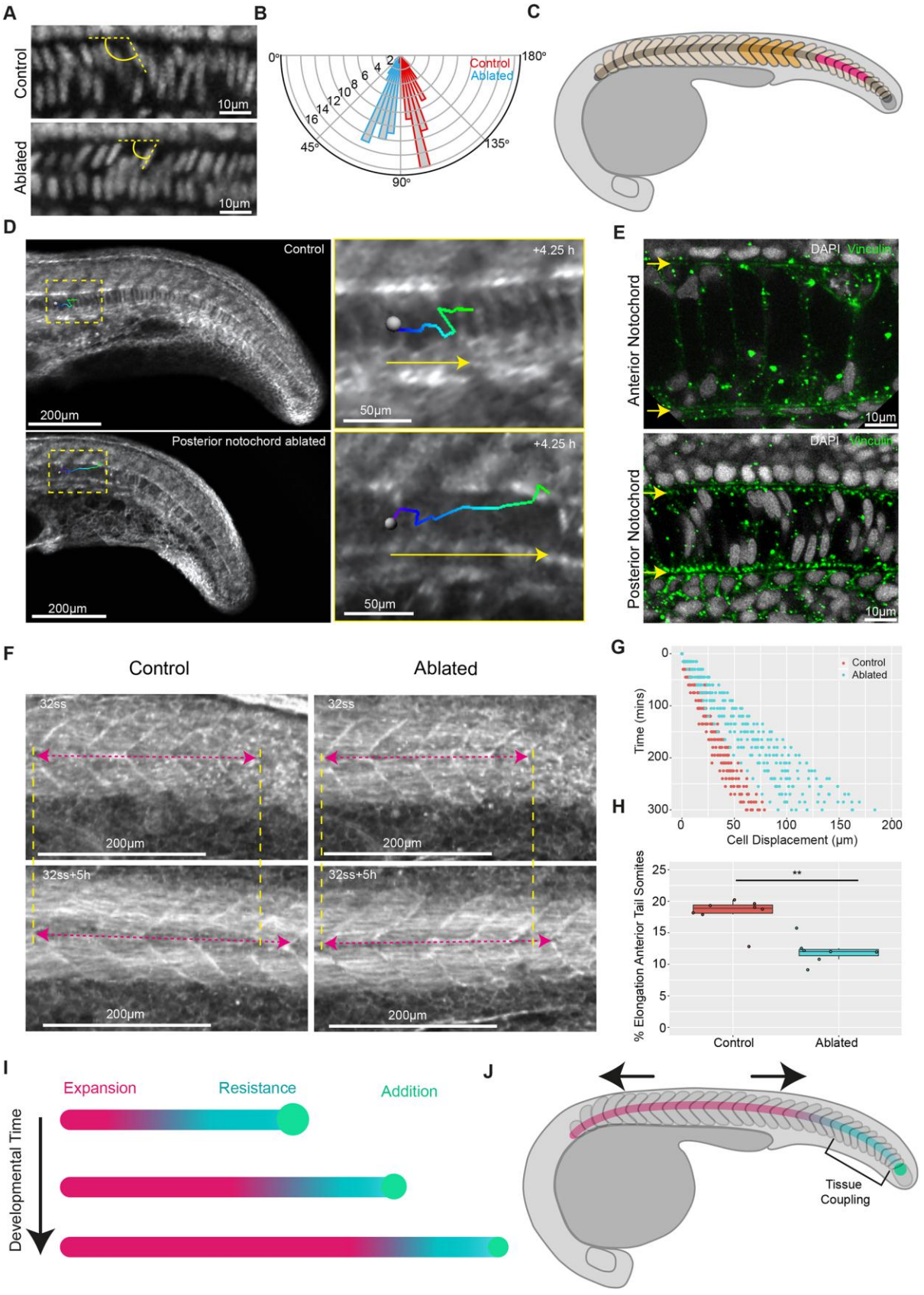

Fig. 4. Notochord progenitors provide a source of resistance to notochord cell expansion, facilitating segmented tissue elongation.

(A) DAPI-stained notochord nuclei located in the anterior tail region in fixed control and ablated embryos.
(B) A polar histogram showing the distribution of angles between dorsally located nuclei and the notochord AP axis (º) in control and ablated embryos (n=12 embryos per condition, 5 angles measured per embryo, $p<0.001$).
(C) Schematic showing the ablated posterior unexpanded region (magenta) and region used for measuring segmented-tissue elongation (orange).
(D) Manual tracking of expanding notochord cells in a representative control and posteriorly-ablated embryo.
(E) Vinculin and DAPI immunostaining in representative anterior and posterior notochord regions. Yellow arrows mark dorsal and ventral extents of the notochord.
(F) Elongation of a 5-somite region in control and posteriorly-ablated post-tailbud stage embryos.
(G) Notochord cell displacement over time in control and posteriorly-ablated embryos (n=4 and n=5 embryos respectively, 3 tracks per embryo).
(H) Percentage elongation of a 5-somite region in control and posteriorly-ablated embryos (n=8 and n=7 embryos respectively, $p<0.01$).
(I) Notochord cell expansion progresses posteriorly along the axis. Expanding cells push against resisting unexpanded notochord cells added by posterior notochord progenitors – generating a stress along the notochord.
(J) The somitic compartment anterior to the posterior resistance point undergoes an AP stretch.

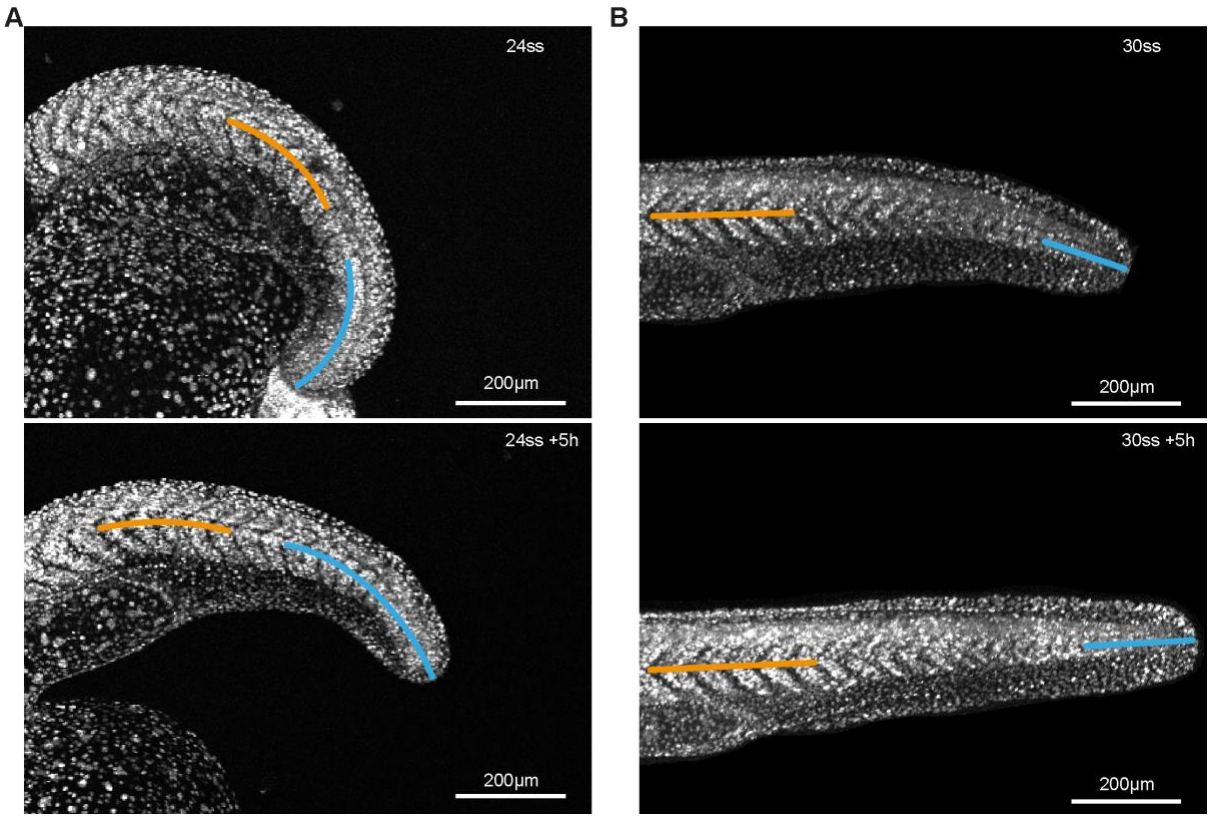

Fig. S1. Segmentation-derived and segmented tissue elongation during tailbud and post-tailbud stages of development.

(A) A live zebrafish embryo expressing NLS-KikGR at the 24-somite stage and 5 hours later.

(B) A live zebrafish embryo expressing NLS-KikGR at approximately the 30-somite stage and 5 hours later.

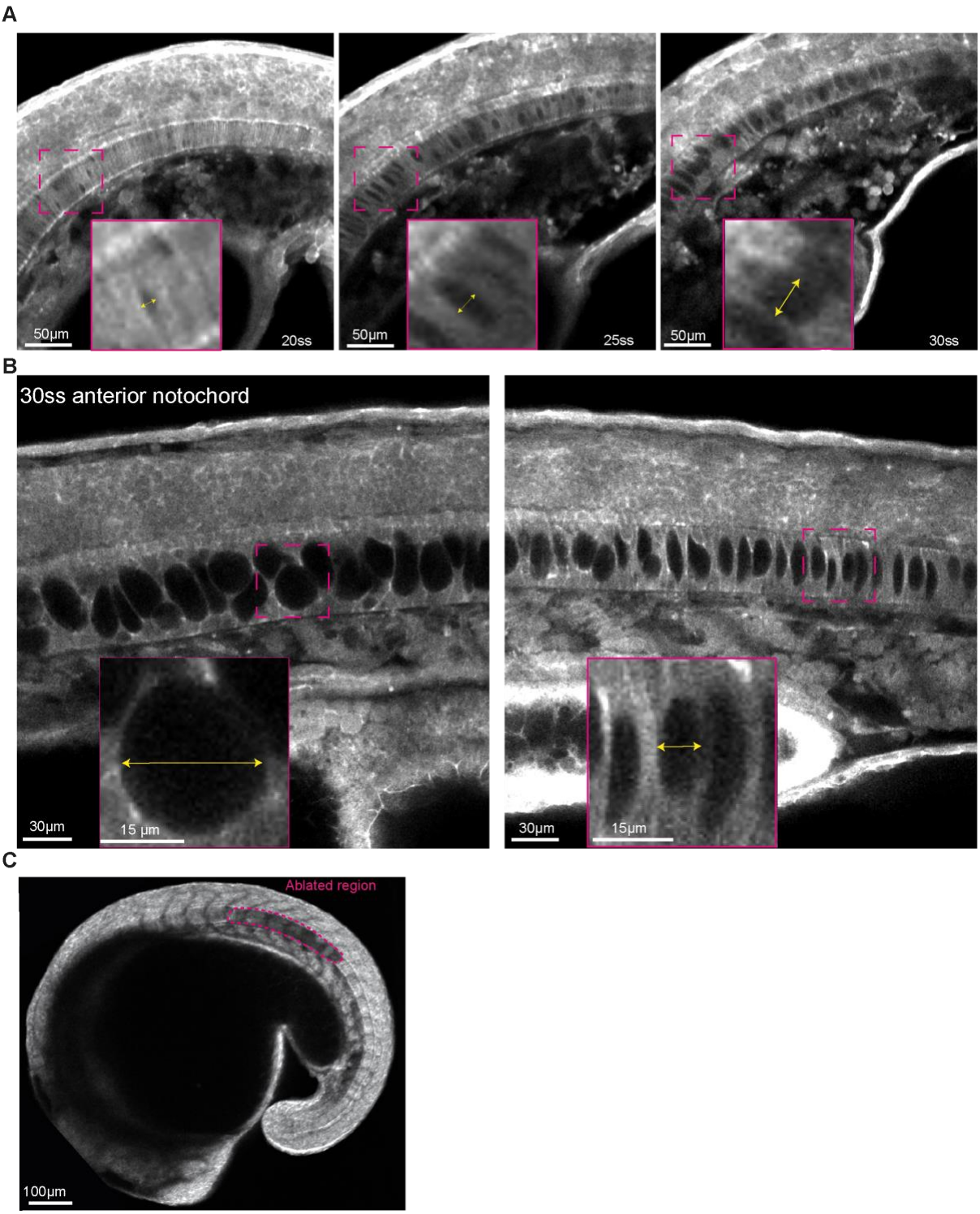

Fig. S2. Notochord cell expansion progresses temporally and spatially along the axis.

(A) Notochord cells in an equivalent region of a Lifeact-GFP expressing embryo at 20, 25, and 30-somite stages. Yellow arrows indicate direction in which length measurements were taken.

(B) Notochord cells in the anterior and posterior of a Lifeact_GFP expressing embryo. Yellow arrows indicate direction in which length measurement was taken.

(C) An anterior notochord ablation in a lifeact-GFP expressing embryo near the onset of vacuolation. Embryos were ablated at 16-18 somite stage.

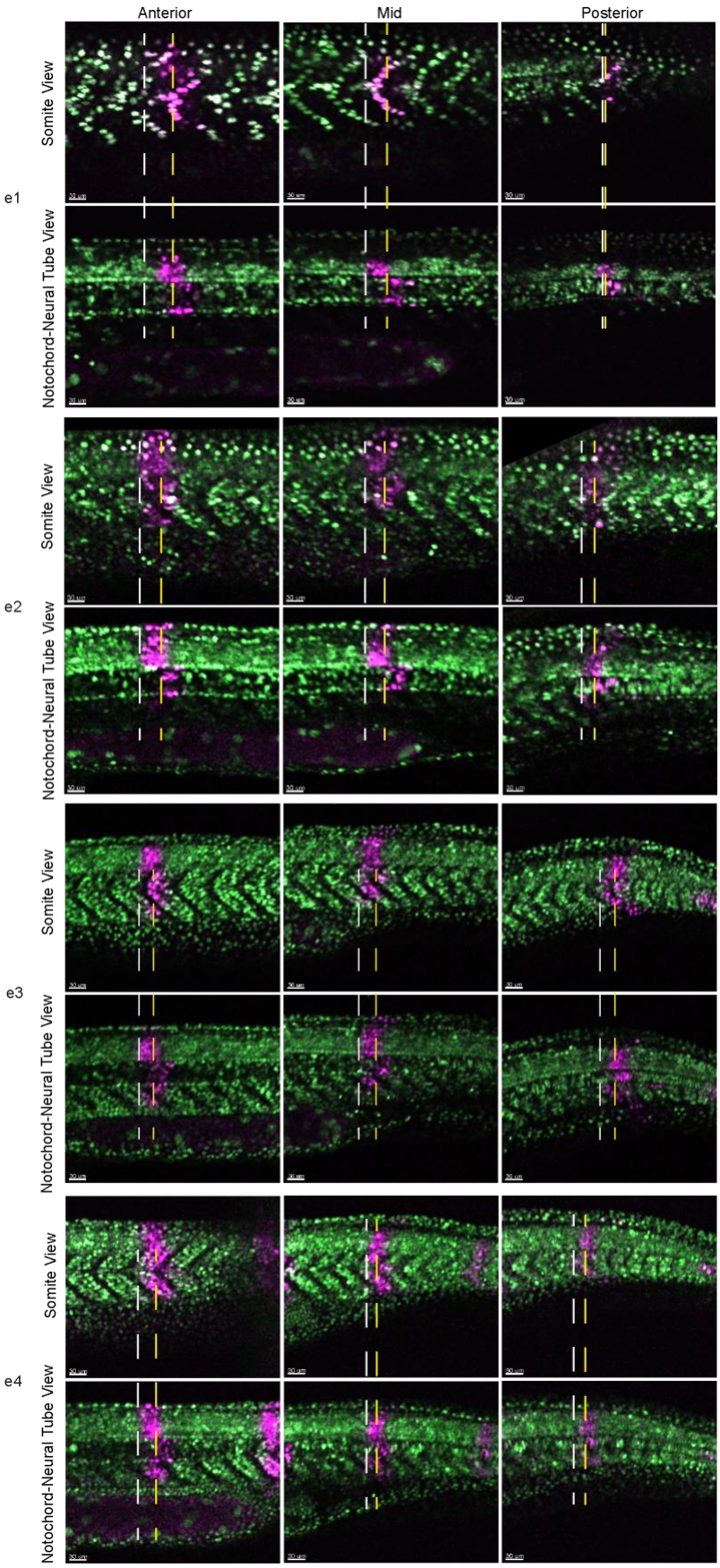

Fig. S3. Notochord and somite label at different regions along the axis in post-tailbud stage embryos.

Images showing the anterior extent of notochord (yellow-line) and somite (white-line) photolabels used to measure the shift between tissues over a 5-hour period.

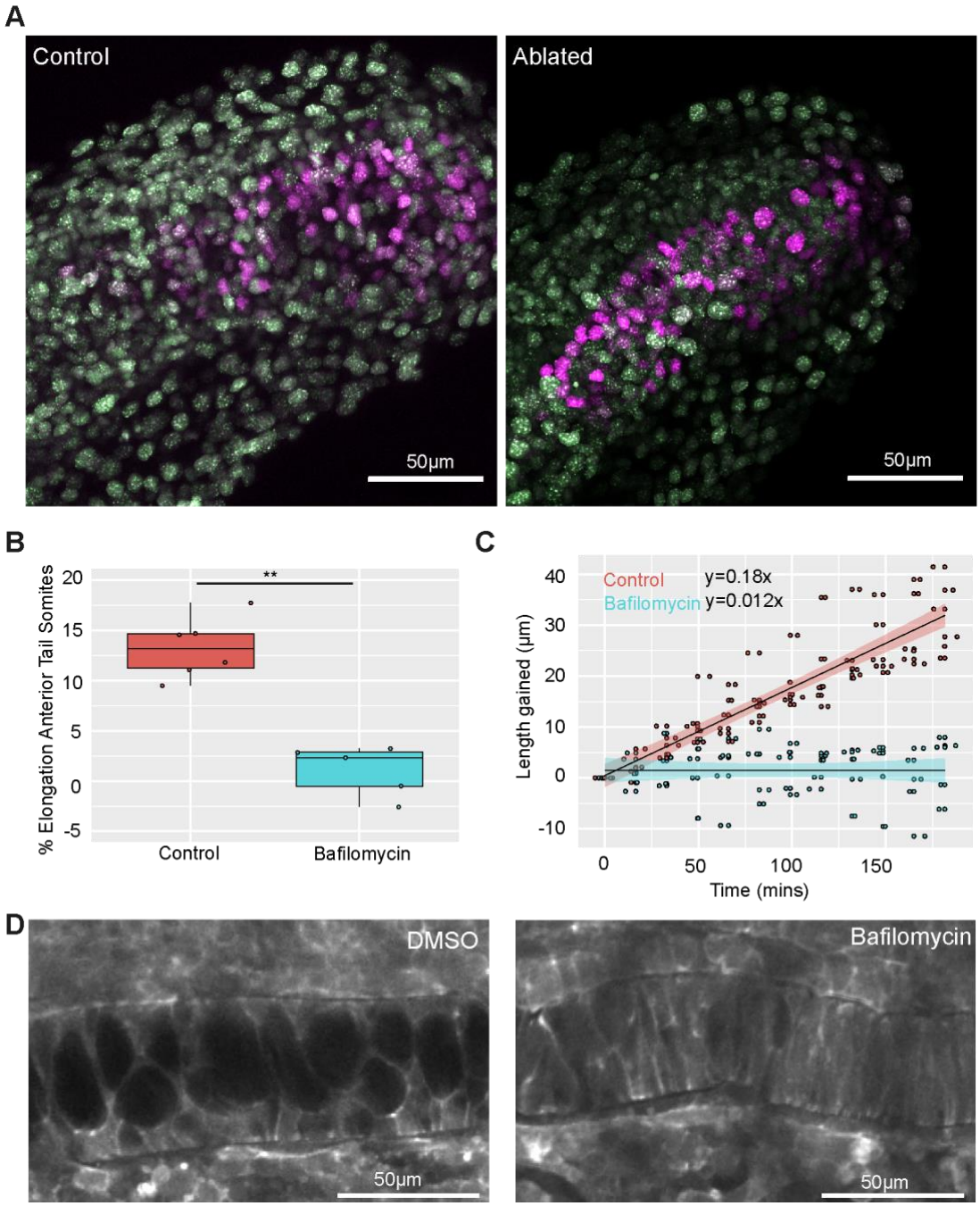

Fig. S4. Disrupted notochord cell expansion impacts segmented tissue-derived, not unsegmented tissue-derived elongation.

(A) Photolabels of presomitic mesoderm progenitors in control and ablated embryos imaged 4 hours after the time of labelling. (n=4 control and n=5 ablated embryos).
(B) Percentage elongation of a 5-somite region over a 3-hour period in DMSO and Bafilomycin treated post-tailbud stage embryos (n=6 control and n=5 Bafilomycin treated embryos, $p<0.01$).
(C) Length gained in a 5-somite region over time in DMSO and Bafilomycin treated embryos (n=6 control and n=5 Bafilomycin treated embryos).
(D) Images of the notochord in DMSO and Bafilomycin treated Lifeact-GFP expressing embryos.

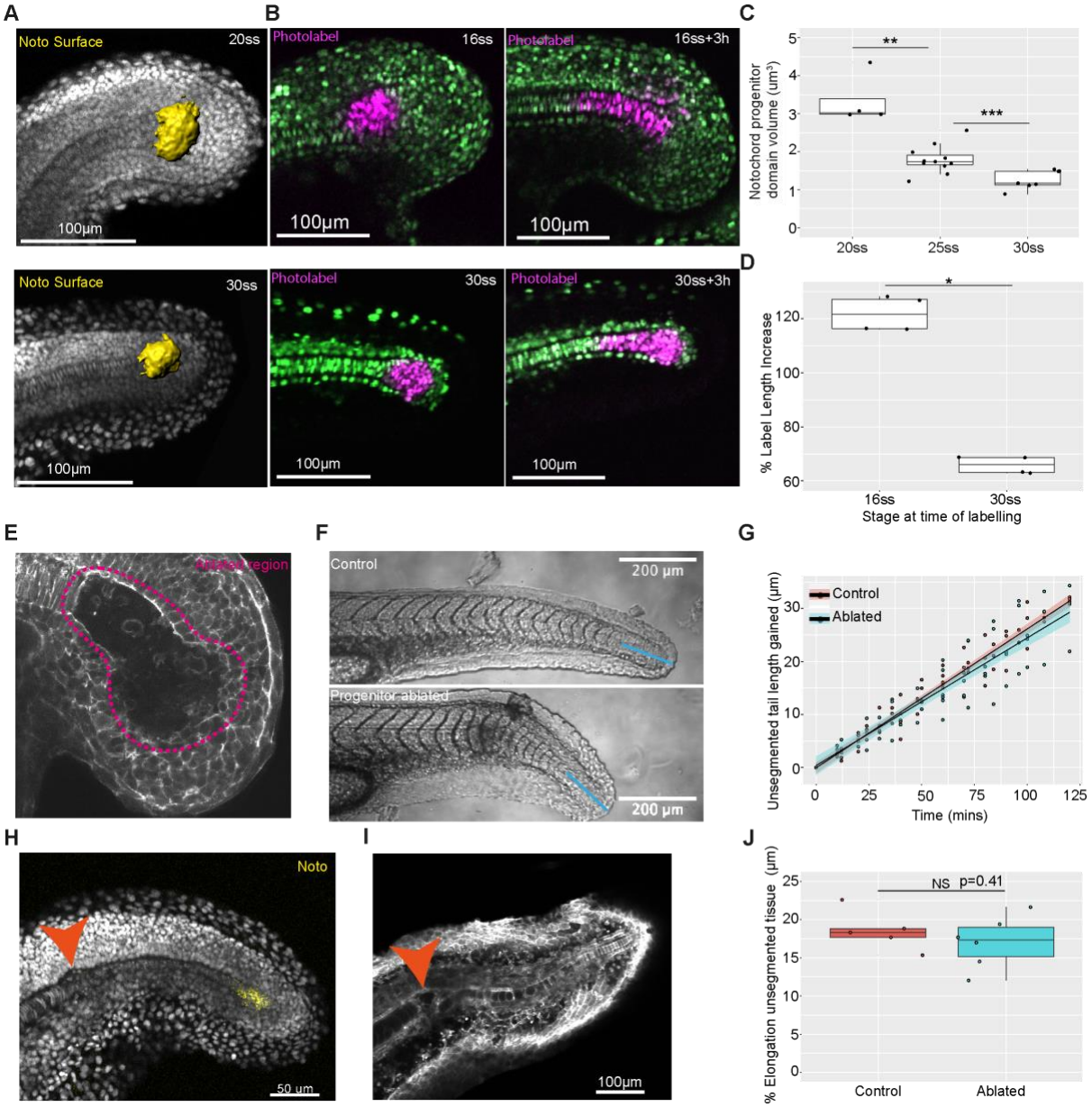

Fig. S5. Notochord progenitors recover after ablation and re-form the posterior notochord.

(A) 3D surfaces of the notochord progenitor domain generated using *Noto* gene expression in 20 and 30 somite stage embryos.
(B) Notochord progenitor photolabels in 16 and 30 somite stage embryos with corresponding images taken 3 hours after labelling.
(C) Notochord progenitor domain volume in 20, 25 and 30 somite stage embryos (n=5, n=13, n=7 embryos respectively, p<0.01, p<0.001 respectively).
(D) Photolabel AP length increase over 3 hours in 16 and 30 somite stage embryos (n=4 embryos per stage, p<0.05).
(E) Representative image of a 16-somite stage embryo with notochord progenitors ablated.
(F) Representative images of control and progenitor ablated post-tailbud stage embryos. The blue line indicates the region of residual unsegmented tissue tracked over time.
(G) Length gain in a small region of unsegmented tissue over time in control and progenitor ablated post-tailbud stage embryos (n=6 control and n=7 ablated embryos).
(H) Representative image of an embryo fixed approximately 5 hours after notochord progenitor ablation. The gene expression marker '*Noto*' marks the notochord progenitors.
(I) Representative image of an embryo imaged approximately 24 hours after notochord progenitor ablation. The recovered notochord is visualised using a lifeact-GFP reporter.
(J) Percentage elongation of unsegmented tissue in the tail region after recovery from notochord progenitor ablation over approximately 100 minutes (n=5 control and n=6 ablated embryos, p=0.41).
Orange arrows indicate the internalised ablated tissue.

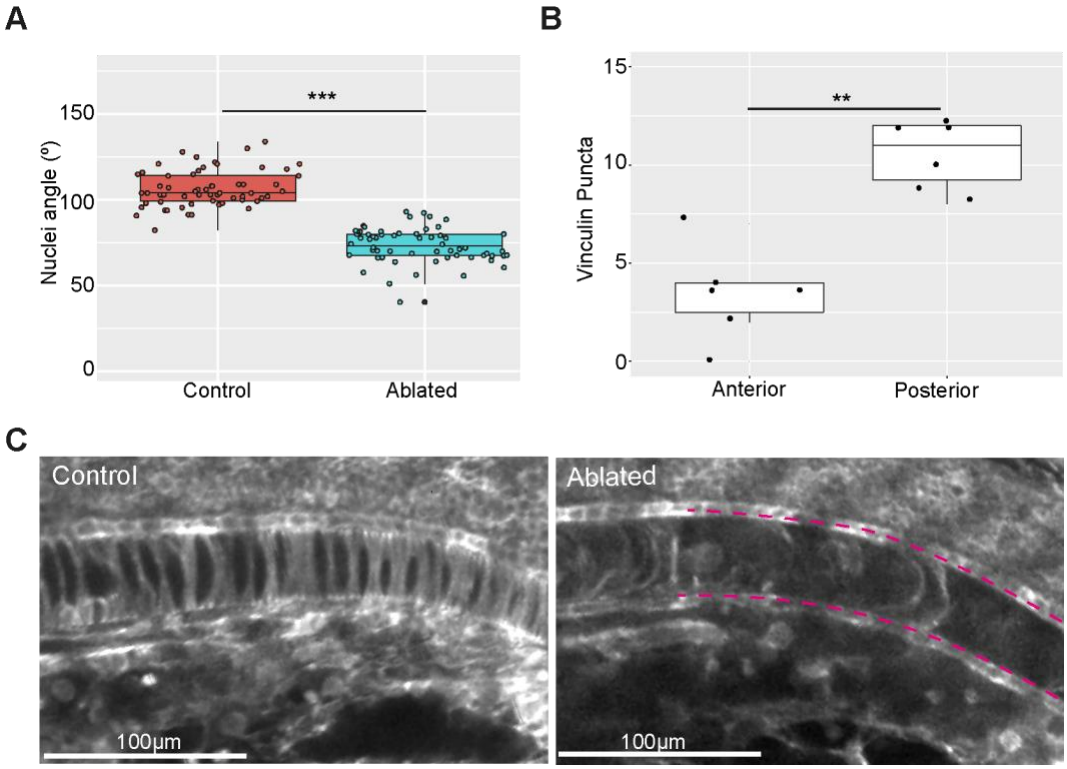

Fig. S6. Unexpanded posterior notochord cells resist anterior cell expansion.

(A) Angles between dorsally located nuclei and the notochord AP axis (º) in control and ablated embryos (n=12 embryos per condition, 5 angles measured per embryo, $p<0.001$).
(B) The number of vinculin puncta present at a notochord-ECM sheath interface in the anterior and posterior (n=3 embryos, 2 interfaces measured per embryo).
(C) Notochord cells located close to the end of the yolk extension in Lifeact-GFP expressing control and posteriorly-ablated embryos (magenta lines).

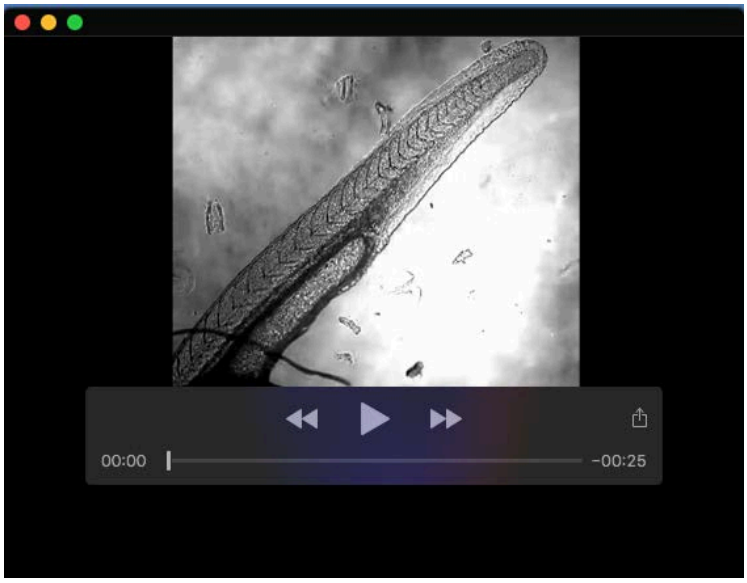

Movie 1. Tailbud and post-tailbud stages of development. A brightfield movie showing embryos transitioning from tailbud to post-tailbud stages of elongation. Time is in minutes.

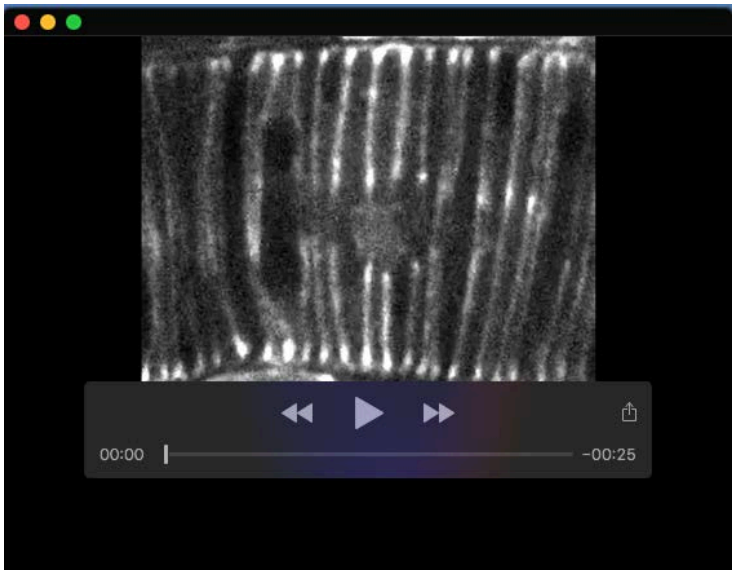

Movie 2. Notochord cell ablation. Multi-photon ablation of notochord cells in a lifeact-GFP expressing embryo.

Movie 3. Vacuolated cell movement in control and anterior-ablated embryos. Movement of expanding vacuolated cells in a control embryo and an embryo with an anterior notochord ablation. Time is in hours.

Movie 4. Vacuolated cells move into the ablated space. Movement of expanding vacuolated cells on either side of an anterior notochord ablation. Time is in hours.

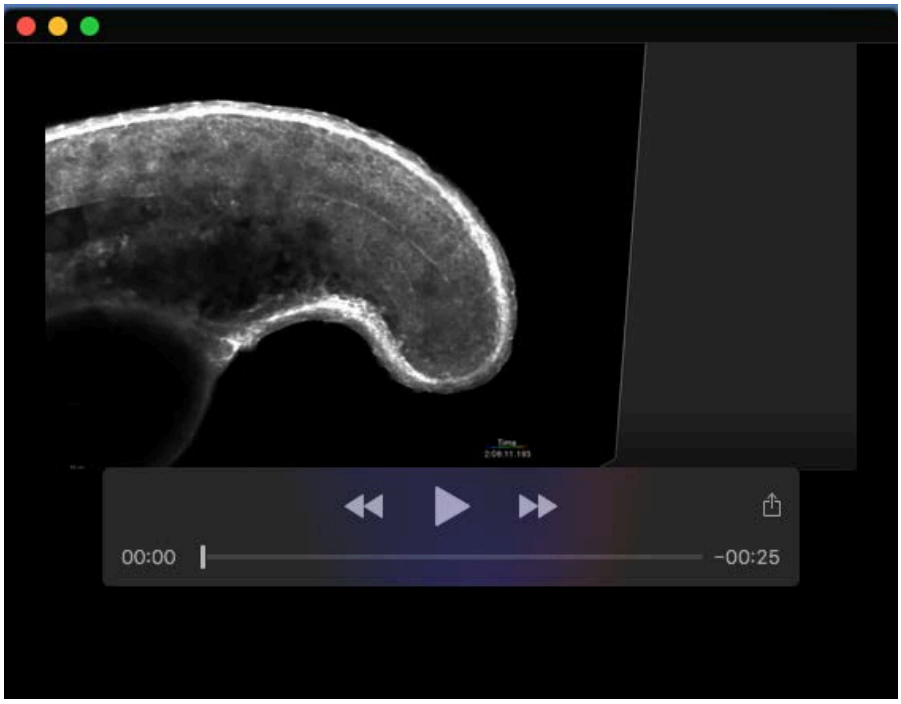

Movie 5. Segmentation-derived elongation is robust to notochord perturbation. Posterior tail elongation in an embryo with an ablation extending into the posterior notochord. Time is in hours.

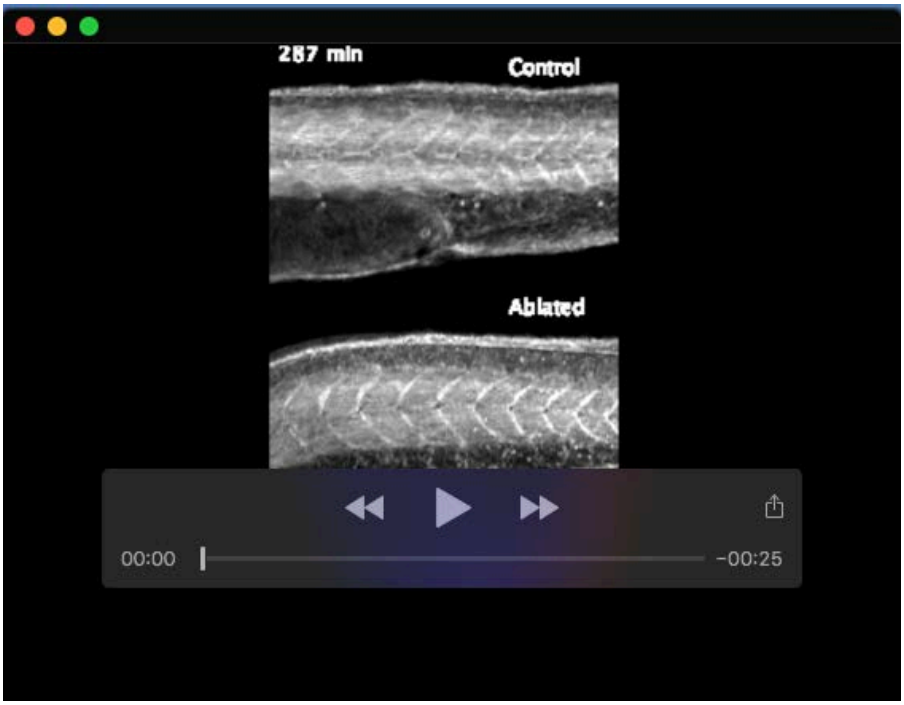

Movie 6. Segmented tissue elongation is decreased in embryos with disrupted notochord cell expansion Elongation of a region of 5 somites in a control and ablated embryo. Time is in minutes.

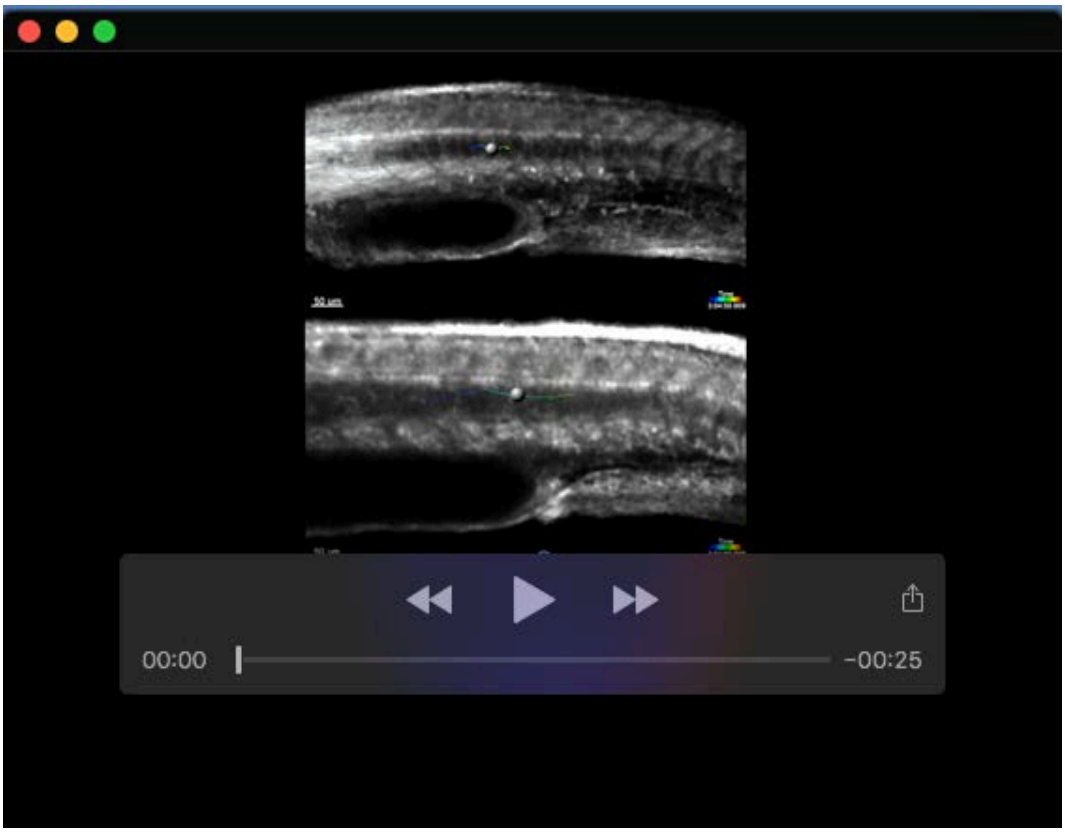

Movie 7. Vacuolated cells move faster when posterior unexpanded cells are removed. Movement of expanding vacuolated cells in a control embryo and an embryo with a posterior notochord ablation. Time is in hours.